# DYNAMIC CONTRAST-ENHANCED MRI IN DETERMINING HISTOLOGICAL TYPE OF CERVICAL CANCER

Tarachkova EV[1] ✉, Shorikov MA[1,2], Panov VO[1,2], Kuznetsov VV[2], Tyurin IE[1,2], Shimanovsky NL[3]

[1] Department of Roentgenology and Radiology,
Russian Medical Academy of Postgraduate Education, Moscow, Russia

[2] Blokhin Russian Cancer Research Center, Moscow, Russia

[3] P. V. Sergeev Molecular Pharmacology and Radiobiology Department, Biomedical Faculty,
Pirogov Russian National Research Medical University, Moscow, Russia

Knowing the histology of cervical cancer (squamos cell carcinoma or adenocarcinoma) is important in deciding on the best treatment plan. We have studied the role of dynamic contrast-enhanced magnetic resonance imaging in the differential diagnosis of cervical cancer. We examined 90 patients between 23 and 78 years of age (mean age was 43.5 years) with histologically distinctive stage IIb–IVb cervical cancers. Scanning was performed on Magnetom Espree 1.5T and Magnetom Skyra 3.0T scanners (Siemens, Germany) using gadobutrol (Gadavist by Bayer, Germany). On T1-weighted images, signal intensity and its rate of change were significantly higher for adenocarcinomas compared to squamos cell carcinomas ($p < 0.04$) from the 20$^{th}$ second after gadobutrol had been delivered to the tumor. With squamos cell carcinomas, the time-intensity curve (showing the dependence of signal intensity on the time elapsed after gadobutrol had been delivered to the tumor) had two phases: a short phase of a relatively slow accumulation of the contrast agent with the subsequent plateau or even signal intensity reduction. The pattern of gadobutrol accumulation allows differentiating between histological types of tumors. Based on the resulting curves, a pharmacokinetic model can be described for each tumor type. Postcontrast images are useful in determining tumor differentiation grade. Specifically, the signal from a well-differentiated adenocarcinoma is the most inhomogeneous one ($p < 0.03$). The method described in this work does not imply that histological analysis is unnecessary and can be recommended as a supplementary diagnostic tool.

**Keywords:** magnetic resonance imaging, contrast enhancement, gadobutrol, cervical cancer, adenocarcinoma, squamos cell carcinoma, differential diagnosis

✉ **Correspondence should be addressed:** Elena Tarachkova
ul. Barrikadnaya, d. 2/1, str. 1, Moscow, Russia, 123995; doctorkid@yandex.ru

**Received:** 10.08.2016 **Accepted:** 18.08.2016

# ВОЗМОЖНОСТИ ДИНАМИЧЕСКОЙ МРТ С КОНТРАСТНЫМ УСИЛЕНИЕМ В ОПРЕДЕЛЕНИИ ГИСТОЛОГИЧЕСКОГО ТИПА РАКА ШЕЙКИ МАТКИ

Е. В. Тарачкова[1]✉, М. А. Шориков[1,2], В. О. Панов[1,2], В. В. Кузнецов[2], И. Е. Тюрин[1,2], Н. Л. Шимановский[3]

[1] Кафедра рентгенологии и радиологии,
Российская медицинская академия последипломного образования, Москва

[2] Российский онкологический научный центр имени Н. Н. Блохина, Москва

[3] Кафедра молекулярной фармакологии и радиобиологии имени акад. П. В. Сергеева, медико-биологический факультет,
Российский национальный исследовательский медицинский университет имени Н. И. Пирогова, Москва

Определение гистологического типа рака шейки матки (плоскоклеточный рак или аденокарцинома) способствует выбору наиболее эффективной терапии. В работе описан метод дифференциальной диагностики заболевания с использованием динамической магнитно-резонансной томографии с контрастным усилением. Были обследованы 90 пациенток в возрасте 23–78 лет (средний возраст — 43,5 года) с гистологически подтвержденным раком шейки матки стадий IIb–IVb. Сканировали на аппаратах Magnetom Espree 1.5T и Magnetom Skyra 3.0T (Siemens, Германия), используя гадобутрол («Гадовист», Bayer, Германия). На Т1-взвешенных изображениях интенсивность сигнала и скорость ее изменения, начиная с 20 с после появления гадобутрола в опухоли, были достоверно выше для аденокарцином, чем для плоскоклеточного рака ($p < 0,04$). При этом для плоскоклеточного рака наблюдали две фазы на кривых зависимости интенсивности сигнала от времени после появления гадобутрола в опухоли: короткую фазу относительно медленного накопления контрастного вещества с последующим выходом на плато или даже снижением сигнала к концу наблюдения (125 с). Именно характер накопления гадобутрола позволяет различать гистологические типы опухолей, и на основе соответствующих кривых могут быть предложены фармакокинетические модели для опухолей разных типов. Постконтрастные изображения полезны для определения степени дифференцировки опухоли. В частности, сигнал от высокодифференцированных аденокарцином достоверно наиболее неоднородный ($p < 0,03$). Описанный метод не исключает гистологической верификации диагноза и может быть рекомендован как дополнительный диагностический инструмент.

**Ключевые слова:** магнитно-резонансная томография, контрастное усиление, гадобутрол, рак шейки матки, аденокарцинома, плоскоклеточный рак, дифференциальная диагностика

✉ **Для корреспонденции:** Тарачкова Елена Владимировна
123995, г. Москва, ул. Баррикадная, д. 2/1, стр. 1; doctorkid@yandex.ru

**Статья получена:** 10.08.2016 **Статья принята в печать:** 18.08.2016

Cervical cancer (CC) remains a troubling health issue among women of reproductive age [1–6]. About 70–80 % of patients with invasive CC are diagnosed with squamous cell carcinoma; 10–20 % are diagnosed with adenocarcinoma [6, 7]. Adenocarcinomas tend to grow more aggressively, form distant metastases more frequently, demonstrate lower five-year survival rates, and require an alternative approach to treatment, specifically, when deciding on chemotherapy drugs [8]. Knowing CC histologic type would ensure timely and effective treatment.

Compared to CT and PET-CT, magnetic resonance imaging (MRI) has some advantages in detecting and staging localized CC; in case of advanced CC, CT and MRI are equally effective. PET-CT is recommended for the detection of recurrences and metastases in lymph nodes [1, 9, 10]. To differentiate between benign and malignant tumors, dynamic contrast-enhanced MRI (DCEMRI) is widely used [1]; however, this technique has not yet been applied to assess CC histologic types. To attempt such assessment, diffusion weighted MR images (DWIs) and apparent diffusion coefficient maps (ADC-maps) were used [11, 12]. Now, we hypothesized that DCEMRI images can be of a higher diagnostic value in the preoperative assessment of the histologic type of cervical cancer (squamous cell carcinoma or adenocarcinoma) and, possibly, tumor grade, compared to DWIs and ADC-mapping or T2-weighted images. Our work addresses the following objectives:

– detecting differences between DCEMRI-based intensity curves of gadobutrol accumulation for various histologic types of CC;

– detecting differences in the intensity and homogeneity of signals from various histologic types of tumor tissues using delayed postcontrast DCEMRI images;

– detecting differences in the signal intensity between various histologic types of CC using fat-suppressed and fat-unsuppressed T2WIs;

– estimating sensitivity and specificity of DCEMRI in the assessment of CC histologic type and grade.

## METHODS

The study was carried out at N. N. Blokhin Russian Cancer Research Center. It enrolled 90 women aged 23–78 (mean age of 43.5 years) with histologically confirmed IIb–IVb cervical cancer, median lesion volume of 43.3 $cm^3$ (22.6 and 92.9 are the 1st and 3rd quantiles, respectively). Patients were distributed into groups depending on CC histologic type and tumor grade, as shown in table 1. Differences in age and lesion volumes between the groups were statistically insignificant ($p > 0.05$).

The following inclusion criteria were applied: suspicion of CC and a need for an adequate treatment plan in confirmed cases; a verified diagnosis of CC requiring a subsequent determination of tumor size, invasion depth, parametrial infiltration, and damage to lymph nodes and surrounding tissues; elevated levels of squamous cell carcinoma antigen (SCCA) in patients with ambiguous results of transvaginal ultrasound examination. Exclusion criteria were as follows: poor general condition of a patient (somatic and pshycic health) that prevented her from lying still during the scan; hypersensitivity to the components of magnetic resonance contrast agents (MRCAs); metal implants or implanted electronic devices (clips, pacemakers); claustrophobia; serious cardiovascular conditions; renal insufficiency (glomerular filtration rate of <30 ml/min); liver failure; patient's weight exceeding the maximum weight capacity of the MRI bed.

The patients were asked to stop eating gas-producing foods two days before the scan. A day before the scan, they were asked to take a standard dose of a laxative, and/or were administered an edema 12 h before the procedure. On the day of the examination, the patients were allowed to have a light breakfast rich in carbohydrates and a minimal amount of liquid (no later than 2 h before the examination). The patients took 40–80 mg of an antispasmodic (drotaverine marketed as No-Spa, by Research Institute of Organic Intermediates and Dyes, Russia) *per os* or, if they were not prone to constipation, 10 mg of hyoscine butylbromide, an antiperistaltic drug (Buscopan Boehringer Ingelheim, Germany). The patients were asked to have their urinary bladder filled with only a small amount of fluid for the scan.

Scans were carried out on Magnetom Espree 1.5T and Magnetom Skyra 3.0T scanners (Siemens, Germany) using a multichannel 12-element receiver body coil placed on the pelvis and centered 2–3 cm above the pubis, with patients in the supine position. The following axial image types were used:

1. fat-unsuppressed T2-weighted images (T2WIs);
2. fat-suppressed T2WIs;

**Table 1.** Distribution of patients with cervical cancer into groups according to tumor histologic type and grade

| Parameter | Squamous cell carcinoma | | | Adenocarcinoma | | |
|---|---|---|---|---|---|---|
| Number of patients | 74 | | | 16 | | |
| Median age (quantile 1, quantile 3), years | 42 (36; 50) | | | 54 (39; 54) | | |
| Median lesion volume (quantile 1, quantile 3), $cm^3$ | 43.6 (22,3; 95,2) | | | 42.2 (24.4; 89.4) | | |
| | Tumor grade | | | | | |
| | low | intermediate grade | high | low | intermediate grade | high |
| Number of patients | 24 | 22 | 6 | 5 | 5 | 5 |
| Median age (quantile 1, quantile 2), years | 37 (35; 43) | 44 (37; 48) | 38 (35; 41) | 59 (54; 62) | 45 (39; 48) | 56 (39; 58) |
| Median lesion volume (quantile 1, quantile 2), $cm^3$ | 43,6 (36.5; 114.6) | 57.6 (40.2; 211.9) | 63,6 (19.8; 166.3) | 87,9 (56.4; 206.1) | 38,2 (30.1; 72.1) | 54,7 (35.3; 74.2) |
| FIGO stage FIGO IIa, % | 28.6 | 33.3 | – | – | 50.0 | 50.0 |
| FIGO stage FIGO IIIa, % | 19.0 | 27.8 | 80.0 | – | – | 50.0 |
| FIGO stage FIGO IIIb, % | 23.8 | 27.8 | 20.0 | 75.0 | 25.0 | – |
| FIGO stage FIGO IVa, % | 19.0 | 5.6 | – | – | – | – |
| FIGO stage FIGO IVb, % | 9.5 | 5.6 | – | 25.0 | 25.0 | – |

**Note.** Lesion volume was measured directly (the sum of tumor square areas on T2-weighted images multiplied by section thickness). Grading was performed in 67 patients.

3. fat-suppressed DWIs with automatic ADC-mapping based on b-factor values of 50, 800 and 1000;

4. unenhanced T1-weighted images (T1WIs);

5. frequency-selective fat-suppressed T1WIs obtained during DCEMRI (keyhole imaging) [13], 35 series of 4.8 s each, in total. To reduce the contribution of fat-suppressed signal heterogeneity and to accurately detect MRCA accumulation zone, unenhanced images were subtracted from MRCA-enhanced images obtained at different time points after MRCA administration. After MRCA was delivered to the tumor, the observation lasted for 125 s;

6. fat-suppressed delayed T1WIs obtained 3–4 minutes after MRCA administration.

Technical parameters of the used sequences are shown in table 2.

For DCEMRI, the patients received a 7.5 ml injection of 1.0 M water-soluble extracellular MRCA gadobutrol (Gadovist by Bayer, Germany), which is about 0.1 mmol/kg of a patient's weight, at a rate of 2.5–3.0 ml/s. Double concentration of gadolinium in this formulation allows administering a lower amount of this drug and still obtaining high quality images, as gadolinium is highly reactive [14]. Gadobutrol is a macrocyclic gadolinium-containing formulation with a low risk of inducing nephrogenic systemic fibrosis [15].

The following parameters were evaluated using MR images:

• signal intensity, i. e., how bright or dark the object is, compared to the surrounding tissues; besides, during quantitative analysis, mean signal intensity (SI) in the region of interest (ROI) was measured (in arbitrary units);

• signal heterogeneity, i.e., non-uniformity of the object's signal distribution against the surrounding tissues; during quantitative analysis, we also assessed the range of signal intensity values within ROI. Those values can be treated as the absolute standard deviation of signal intensity (SDOSI, a. u.) or a ratio of standard deviation to signal intensity (a nondimensional value) within ROI.

According to the description, these parameters are available for simple visual assessment. However, we can also find their reference range using a standard interface of the workstation. To measure changes in signal intensity on all image types, we used SI and SDOSI data from the manually selected ROIs of cervical cancer tissue and gluteus maximus muscle (MR signal was normalized to the muscle signal from regions no bigger than 15 pixels in size). Thus, signal intensity was additionally evaluated as a ratio of SI in the tumor region to muscle SI.

After subtracting unenhanced MR-images from enhanced MR-images, we built time-curves based on DCEMRI data (fig. 1) showing changes in SI and its SD and calculated SI and SD in the same areas using postcontrast images obtained in the delayed phase. For each curve, a point of inflexion was determined, past which the rate of MRCA accumulation changed. We drew tangent lines to the initial and finishing curve segments, and their intersection point was considered an inflexion point (a point where the rate of signal intensity changes). Because the position of the inflexion point varied, it was taken as zero time point t for further calculations. However, the tables in this article show time elapsed after gadobutrol delivery to the tumor. Relative signal intensity, RSI(t), was calculated according to the following formula:

$$RSI(t) = \frac{SI(t) - SI(0)}{SI(0)} \times 100\ \%,$$

where RSI(t) is relative signal intensity at a given time point *t* after the inflextion point; SI(0) is signal intensity at inflexion point, SI(t) is signal intensity at a given time point *t* (here, we use *t* = 15, 30, 60 and 110 s after the inflexion point).

Statistical processing was done using Miscrosoft Excel 10 software with Addinsoft XLStat addon (Addinsoft, USA) and Statistica 10.0 (StatSoft, USA) using Mann–Whitney, Kruskal–Wallis and Dunn tests and ROC (reciever operator curves) analysis. The study was approved by the Research Ethics Committee of the Russian Medical Academy of Postgraduate Education (Protocol 8 dated June 14, 2016).

## RESULTS

After MRCA administration, we observed a 10–20 s period (median of 15 s) of rapid and vigorous accumulation of the contrast agent in tumors of both types, with a corresponding change in SI after gadobutrol delivery to the tumor (fig. 2). This phase ended at the inflexion point of the time-SI curve. Past this point, adenoarcinomas exhibited a more intense MR-signal change followed by a more rapid uniform accumulation of gadobutrol ($p < 0.003$–$0.040$). For squamous cell carcinomas, MR signal intensity was lower 15 s after MRCA administration;

**Table 2.** MR-sequences used in the study and their parameters

| Image type | Fat suppression | Sequence type and extra parameters | Slice thickness, mm | Field of view (side), mm | Matrix, pixel x pixel | TR/TE, ms | Number of accumulations |
|---|---|---|---|---|---|---|---|
| T2WI | No suppression or frequency-selective suppression | Turbo spin echo, acceleration factor is 17 | 3 | 320 | 384 x 384 | 6300–8000/132 | 1 |
| DWI + ADC-maps | Selective suppression with inverting pulse | Echoplanar imaging, diffusion weighted imaging b-value is 50, 800, 1000 | 3–4 | 400 | 96 x 196 | 370/82 | 6 |
| T1WI before MRCA injection, T1WI after MRCA injection in the delayed phase (3–4 minutes after the injection) | Frequency-selective suppression | Volumetric interpolated examination, flip angle is 10° | 2 | 240 | 243 x 320 | 5.94/2.08 | 1 |
| DCEMRI T1WI | Frequency-selective suppression | Time resolved imaging with stochastic trajectories, flip angle is 12°, k-space central and peripheral acquisition A is 51 % and B is 21 %, total observation time is 125 s | 3 | 260 | 192 x 256 | 466/186 | 1 |

for the time-SI curve, two phases were typical: a short phase of relatively slow accumulation of the contrast agent (60 s past the inflexion point or 15 to 75 s after gadobutrol delivery to the tumor) with subsequent plateau or even MR signal reduction observed at second 125 after gadobutrol delivery to the tumor.

Differences between adenocarcinoma and squamous cell carcinoma detected during the analysis of SI and SDOSI on fat-suppressed T2WIs and then on T1WIs obtained during DCEMRI and in the delayed phase after MRCA administration are shown in tables 3 and 4. On fat-suppressed T2WIs, adenomas are characterized by a more intense and more homogenous signal, compared to squamous cell carcinomas ($p < 0.03–0.05$). With DCEMRI, SI and its rate of change on T1WIs were significantly higher for adenocarcinomas ($p < 0.003–0.040$) 20 s after gadobutrol had been delivered to the tumor and thereafter. On postcontrast images obtained during the delayed phase, poorly differentiated adenocarcinomas are characterized by a more homogenous signal compared to moderately and well-differentiated adenocarcinomas and squamous cell carcinomas of any grade, while for well-differentiated adenocarcinomas, a more heterogenous signal is typical, compared to adenocarcinomas and squamous cell carcinomas of any grade ($p < 0.03$). No significant differences were found for squamos cell carcinomas.

Due to an additional inflexion point appearing on the squamous cell carcinoma curve (around second 75 after gadobutrol delivery to the tumor), we also assessed the ratio of signal intensity at this time point to signal intensity at the end point (second 125). For squamous cell carcinoma, this ratio was close to 1 (plateau), for adenocarcinoma it was 1.1 ($p < 0.02$). This parameter and relative signal intensity 75 s after gadobutrol delivery to the tumor turned to be the most sensitive and specific (table 3). With optimized accuracy (a maximum sum of sensitivity and specificity), it was 0.75 for tumors of both types.

ROC-analysis also confirmed that specifics of gadobutrol accumulation best characterize the histologic type of a tumor. Additional parameters that were significantly different for adenocarcinomas and squamous cell carcinomas obtained from fat-suppressed T2WIs (SI absolute value, SI of the tumor normalized to the SI of the gluteus, and SDOSI) must be considered secondary. To understand their contribution, a model was built based on the binary logistic regression. It allowed for the assessment of total sensitivity and specificity of the method while using a combination of parameters: after frequency optimization, their values for adenocarcinoma were 0.80 and 0.86, respectively, and for squamous cell carcinoma — 0.86 and 0.80, respectively.

Postcontrast images in the delayed phase were useful in the assessment of tumor grade: they allow for highly sensitive and specific discrimination between poorly and well-differentiated adenocarcinomas. The former are characterized by a more homogenous signal; their sensitivity and specificity for a 0.90 area under ROC curve are 0.75 and 0.96, respectively. The latter are characterized by a more heterogeneous signal and are detected with 1.00 sensitivity and 0.83 specificity for a 0.88 area under ROC curve.

With ADC mapping, no significant differences were detected between tumors of two studied types of 15–30 pixels in size ($p = 0.21$).

## DISCUSSION

Results obtained by other researchers in quite large samples (80 and 112 patients) demonstrated the possibility of detecting significant differences between adenicarcinomas and squamous cell carcinomas of various grades using the ADC mapping technique [11, 12]. The authors emphasize that MRI scans can contribute to a more accurate diagnosis or verify histological data, thus preventing medical errors. However, in both experiments mean ADC was calculated for the entire tumor, meaning that each slice where cervical cancer was detected had to be processed. This kind of analysis is quite time-consuming and can hardly be recommended for clinical use even in big specialized centers. We failed to establish a connection between ADC and tumor histologic type using a simpler measurement technique (ROI of 15–30 pixels). Besides, an accurate and precise ADC map is difficult to reproduce and construct, especially when only 2 or 3 b-factor values [16–18]. Our technique is simpler and easy to apply. DCEMRI here matters not only for the diagnosis but for the prognosis of CC outcome. Lund et al. [19] report low levels

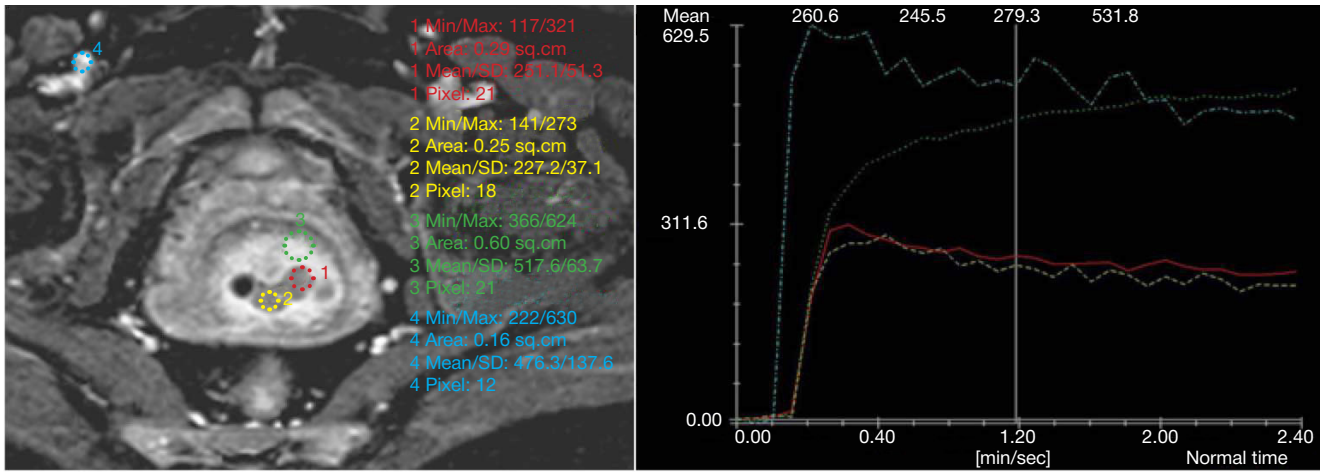


**Fig. 1.** Magnetic resonance contrast agent accumulation curves obtained on the scanner workstation

An axial section is on the left, obtained from a dynamic contrast-enhanced MR image (80 s after scanning was launched) of a patient with squamous cell carcinoma. Regions of interest (ROIs) are shown in different colors. The yellow (1) and red (2) circles show cervical cancer, the green (3) circle shows intact myometrium, the blue circle (4) shows a blood vessel. Signal intensity-time curves based on the ROI data are shown on the right. The vertical line designates time elapsed after measurements were started (80 s). The horizontal axis shows time elapsed after contrast agent delivery to the tumor (seconds); the vertical axis shows relative signal intensity. A higher signal intensity is characteristic of intact myometrium and the vessel.

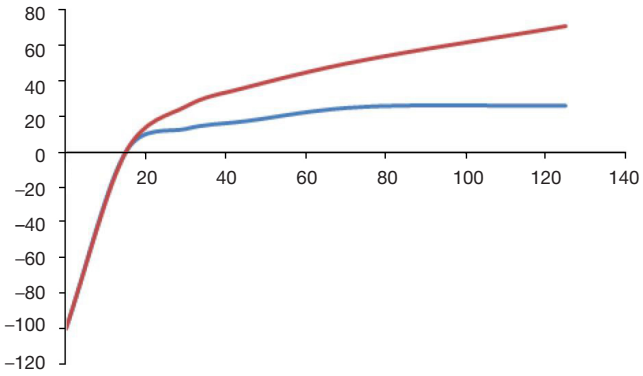


**Fig. 2.** A typical gadobutrol accumulation curve for two types of cervical cancer (squamous cell carcinoma and adenocarcinoma)

The horizontal axis shows time elapsed after contrast agent delivery to the tumor (seconds); the vertical axis shows relative signal intensity in tumor tissue (the red curve shows adenocarcinoma dynamics, the blue curve shows squamous cell carcinoma dynamics).

**Table 3.** Median values and the range of differences between studied parameters on fat-suppressed T2-weighted images and T1-weighted images after gadobutrol injection to the region of interest (no smaller than 15 pixels) for cervical cancer of two histologic types (squamous cell carcinoma and adenocarcinoma)

| Parameter | p-value | Histologic type of cervical cancer | Median, a. u. | Quantile 1, a. u. | Quantile 3, a. u. |
|---|---|---|---|---|---|
| Fat-suppressed T2WI | | | | | |
| Tumor SI | 0.05 | Squamous cell carcinoma | 250.38 | 202.38 | 295.11 |
| | | Adenocarcinoma | 306.57 | 260.3 | 309.35 |
| Tumor SI / Muscle SI | 0.03 | Squamous cell carcinoma | 5.97 | 4.64 | 6.79 |
| | | Adenocarcinoma | 7.17 | 5.37 | 7.81 |
| SDOSI of tumor / SDOSI of muscle | 0.02 | Squamous cell carcinoma | 0.15 | 0.11 | 0.18 |
| | | Adenocarcinoma | 0.11 | 0.09 | 0.15 |
| T1WI obtained during DCEMRI after MRCA administration | | | | | |
| RSI(30) | 0.01 | Squamous cell carcinoma | 12.88 | 4.8 | 23.21 |
| | | Adenocarcinoma | 25.68 | 16.27 | 35.13 |
| RSI(45) | 0.02 | Squamous cell carcinoma | 17.27 | 7.98 | 35.98 |
| | | Adenocarcinoma | 36.40 | 19.18 | 46.51 |
| RSI(75) | 0.005 | Squamous cell carcinoma | 25.38 | 7.23 | 47.73 |
| | | Adenocarcinoma | 52.11 | 33.53 | 66.17 |
| RSI(125) | 0.002 | Squamous cell carcinoma | 25.93 | 6.60 | 69.97 |
| | | Adenocarcinoma | 71.09 | 41.34 | 100.38 |
| SI(125) / SI(75) | 0.02 | Squamous cell carcinoma | 1.00 | 0.94 | 1.08 |
| | | Adenocarcinoma | 1.11 | 1.02 | 1.21 |
| SDOSI(125) | 0.04 | Squamous cell carcinoma | 42.10 | 33.70 | 81.60 |
| | | Adenocarcinoma | 53.70 | 37.2 | 81.60 |
| SDOSI(125) / SI(125) | 0.02 | Squamous cell carcinoma | 0.15 | 0.11 | 0.21 |
| | | Adenocarcinoma | 0.22 | 0.17 | 0.28 |

**Note.** SI is signal intensity; RSI(t) is relative signal intensity on T1-weighted images obtained during dynamic contrast-enhanced MRI at time point *t* (seconds) after gadobutrol delivery to the tumor; SDOSI is standard deviation of signal intensity. Significance of differences was assessed using Mann–Whitney test.

**Table 4.** Median standard deviation of signal intensity and its range on postcontrast T1-weighted images in the delayed phase after gadobutrol injection for cervical cancers of two histologic types (squamous cell carcinoma and adenocarcinoma) and different grades

| Histologic type | Tumor grade | Median SD, a.u. | SD quantile, a.u. | SD quantile 3, a.u. |
|---|---|---|---|---|
| Squamous cell carcinoma | Low | 47.55 | 37.80 | 52.70 |
| | Intermediate | 34.25 | 30.00 | 46.50 |
| | High | 32.10 | 28.70 | 41.40 |
| Adenocarcinoma | Low | 25.65* | 24.95* | 29.75* |
| | Intermediate | 38.30 | 33.20 | 39.00 |
| | High | 57.20* | 56.00* | 68.10* |

**Note.** Significance of differences was assessed using Kruskal–Wallis test and then confirmed by Dunn's paired test. * — $p < 0.03$.

of contrast enhancement during DCEMRI associated with a poorer prognosis, compared to a higher level of enhancement.

Besides, DCEMRI detected differences between MRCA accumulation curves of squamous cell carcinomas and adenocarcinomas. Therefore, it might be possible to build a two-compartment pharmacokinetic model [20] of gadobutrol accumulation (blood-tumor tissue) for adenocarcinoma, and a more complex three-compartment model for squamous cell carcinoma. The latter could be explained by the presence of (or, possibly, partial preservation of) a basement membrane on the inner mucosal layer of the cervix, and this can influence the choice of treatment, as it determines the type of blood circulation and eventually tumor bioaccessibility to chemotherapy drugs.

## CONCLUSIONS

Contrast-enhanced dynamic magnetic resonance imaging allows detecting histologic type of cervical cancer (adenocarcinoma or squamous cell carcinoma) with high accuracy prior to excision using contrast agent accumulation data obtained from T1-weighted images; it also allows detecting adenocarcinoma grade based on the analysis of postcontrast images (in such adenomas, the signal is the most heterogeneous). However, our technique does not exclude the need for biopsy or other types of histological verification of the diagnosis and can be recommended as an additional diagnostic tool only.

### References


1. Bourgioti C, Chatoupis K, Moulopoulos LA. Current imaging strategies for the evaluation of uterine cervical cancer. World J Radiol. 2016; 8 (4): 342–54.
2. Jemal A, Siegel R, Ward E, Hao Y, Xu J, Murray T, et. al. Cancer statistics, 2008. CA Cancer J Clin. 2008; 58 (2): 71–96.
3. Howlader N, Noone A, Krapcho M. SEER Cancer Statistics Review, 1975–2010. 2012. Available from: http://seer.cancer.gov/archive/csr/1975_2010/.
4. Siegel R, Naishadham D, Jemal A. Cancer statistics, 2013. CA Cancer J Clin. 2013; 63 (1): 11–30.
5. Axel EM. [Incidence and mortality from malignant tumors of the female reproductive system in Russia]. Gynecologic Oncology. 2012; (1): 18–23. Russian.
6. Davydov MI, Kuznetsov VV, Nechushkina MV, editors. Lektsii po onkoginekologii. Moscow: MEDpress-inform; 2009. 432 p. Russian.
7. Cervical Cancer Statistics [Internet]. London: Cancer Research UK. [cited 2016 Aug]. Available from: http://www.cancerresearchuk.org/cancer-info/cancerstats/types/cervix/.
8. Williams NL, Werner TL, Jarboe EA, Gaffney DK. Adenocarcinoma of the cervix: should we treat it differently? Curr Oncol Rep. 2015; 17 (4): 17.
9. Tarachkova EV, Streltsova ON, Panov VO, Bazaeva IY, Tyurin IE. [Multiparameter magnetic resonance imaging in the diagnosis of cancer of the cervix uteri]. Vestnik rentgenologii i radiologii. 2015; (6): 43–55. Russian.
10. Trufanov GE, Panov VO. Rukovodstvo po luchevoy diagnostike v ginekologii. Saint-Petersburg: ELBI-SPb; 2008. 592 p. Russian.
11. Kuang F, Ren J, Zhong Q, Liyuan F, Huan Y, Chen Z. The value of apparent diffusion coefficient in the assessment of cervical cancer. Eur Radiol. 2013; 23 (4): 1050–8.
12. Nakamura K, Kajitani S, Joja I, Haruma T, Fukushima C, Kusumoto T, et al. The posttreatment mean apparent diffusion coefficient of primary tumor is superior to pretreatment ADCmean of primary tumor as a predictor of prognosis with cervical cancer. Cancer Med. 2013; 2 (4): 519–25.
13. van Vaals JJ, Brummer ME, Dixon WT, Tuithof HH, Engels H, Nelson RC, et al. Keyhole method for imaging of contrast uptake. J Magn Reson Imaging. 1993; 3 (4): 671–5.
14. Gutierrez JE, Rosenberg M, Seemann J, Breuer J, Haverstock D, et al. Safety and Efficacy of Gadobutrol for Contrast-enhanced Magnetic Resonance Imaging of the Central Nervous System: Results from a Multicenter, Double-blind, Randomized, Comparator Study. Magn Reson Insights. 2015; 8: 1–10.
15. Thomsen HS, Morcos SK, Almén T, Bellin MF, Bertolotto M, Bongartz G, et al. Nephrogenic systemic fibrosis and gadolinium-based contrast media: updated ESUR Contrast Medium Safety Committee guidelines. Eur Radiol. 2013; 23 (2):307–18.
16. Koh DM, Thoeny HC, editors. Diffusion-Weighted MR Imaging: Application in The Body. Springer-Verlag Berlin Heidelberg; 2010, p. 7–16.
17. Giannotti E, Waugh S, Priba L, Davis Z, Crowe E, Vinnicombe S. Assessment and quantification of sources of variability in breast apparent diffusion coefficient (ADC) measurements at diffusion weighted imaging, Eur J Radiol. 2015; 84 (9): 1729–36.
18. Malyarenko DI, Ross BD, Chenevert TL. Analysis and correction of gradient nonlinearity bias in ADC measurements. Magn Reson Med. 2014; 71 (3): 1312–23.
19. Lund KV, Simonsen TG, Hompland T, Kristensen GB, Rofstad EK. Short-term pretreatment DCE-MRI in prediction of outcome in locally advanced cervical cancer. Radiother Oncol. 2015; 115 (3): 379–85.
20. Campbell JL Jr, Clewell RA, Gentry PR, Andersen ME, Clewell HJ. 3rd Physiologically based pharmacokinetic/toxicokinetic modeling. 2012 Computational Toxicology, Methods in Molecular Biology Series: 439–99.


### Литература


1. Bourgioti C, Chatoupis K, Moulopoulos LA. Current imaging strategies for the evaluation of uterine cervical cancer. World J Radiol. 2016; 8 (4): 342–54.
2. Jemal A, Siegel R, Ward E, Hao Y, Xu J, Murray T, et. al. Cancer statistics, 2008. CA Cancer J Clin. 2008; 58 (2): 71–96.
3. Howlader N, Noone A, Krapcho M. SEER Cancer Statistics Review, 1975–2010. 2012. Доступно по ссылке: http://seer.cancer.gov/archive/csr/1975_2010/.
4. Siegel R, Naishadham D, Jemal A. Cancer statistics, 2013. CA Cancer J Clin. 2013; 63 (1): 11–30.
5. Аксель Е. М. Статистика злокачественных новообразований женской половой сферы. Онкогинекология. 2012; (1): 18–23.
6. Давыдов М. И., Кузнецов В. В., Нечушкина М. В., редакторы. Лекции по онкогинекологии. М.: МЕДпресс-информ; 2009. 432 с.
7. Cervical Cancer Statistics [Интернет]. London: Cancer Research UK. [дата обращения: август 2016 г.]. Доступно по ссылке: http://www.cancerresearchuk.org/cancer-info/cancerstats/types/cervix/.
8. Williams NL, Werner TL, Jarboe EA, Gaffney DK. Adenocarcinoma of the cervix: should we treat it differently? Curr Oncol Rep. 2015; 17 (4): 17.
9. Тарачкова Е. В., Стрельцова О. Н., Панов В. О., Базаева И. Я., Тюрин И. Е. Мультипараметрическая магнитно-резонансная томография в диагностике рака шейки матки. Вестник рентгенологии и радиологии. 2015; (6): 43–55.
10. Труфанов Г. Е., Панов В. О., редакторы. Руководство по лучевой диагностике в гинекологии. СПб.: Элби-СПб; 2008. 592 с.
11. Kuang F, Ren J, Zhong Q, Liyuan F, Huan Y, Chen Z. The value of apparent diffusion coefficient in the assessment of cervical cancer. Eur Radiol. 2013; 23 (4): 1050–8.
12. Nakamura K, Kajitani S, Joja I, Haruma T, Fukushima C,

Kusumoto T, et al. The posttreatment mean apparent diffusion coefficient of primary tumor is superior to pretreatment ADCmean of primary tumor as a predictor of prognosis with cervical cancer. Cancer Med. 2013; 2 (4): 519–25.
13. van Vaals JJ, Brummer ME, Dixon WT, Tuithof HH, Engels H, Nelson RC, et al. Keyhole method for imaging of contrast uptake. J Magn Reson Imaging. 1993; 3 (4): 671–5.
14. Gutierrez JE, Rosenberg M, Seemann J, Breuer J, Haverstock D, et al. Safety and Efficacy of Gadobutrol for Contrast-enhanced Magnetic Resonance Imaging of the Central Nervous System: Results from a Multicenter, Double-blind, Randomized, Comparator Study. Magn Reson Insights. 2015; 8: 1–10.
15. Thomsen HS, Morcos SK, Almén T, Bellin MF, Bertolotto M, Bongartz G, et al. Nephrogenic systemic fibrosis and gadolinium-based contrast media: updated ESUR Contrast Medium Safety Committee guidelines. Eur Radiol. 2013; 23 (2):307–18.
16. Koh DM, Thoeny HC, editors. Diffusion-Weighted MR Imaging: Application in The Body. Springer-Verlag Berlin Heidelberg; 2010, p. 7–16.
17. Giannotti E, Waugh S, Priba L, Davis Z, Crowe E, Vinnicombe S. Assessment and quantification of sources of variability in breast apparent diffusion coefficient (ADC) measurements at diffusion weighted imaging, Eur J Radiol. 2015; 84 (9): 1729–36.
18. Malyarenko DI, Ross BD, Chenevert TL. Analysis and correction of gradient nonlinearity bias in ADC measurements. Magn Reson Med. 2014; 71 (3): 1312–23.
19. Lund KV, Simonsen TG, Hompland T, Kristensen GB, Rofstad EK. Short-term pretreatment DCE-MRI in prediction of outcome in locally advanced cervical cancer. Radiother Oncol. 2015; 115 (3): 379–85.
20. Campbell JL Jr, Clewell RA, Gentry PR, Andersen ME, Clewell HJ. 3rd Physiologically based pharmacokinetic/toxicokinetic modeling. 2012 Computational Toxicology, Methods in Molecular Biology Series: 439–99.